Hybrid Density Functional Studies of Pheophytin Anion Radicals: Implications for Initial Electron Transfer in Photosynthetic Reaction Centers

Patrick J O'Malley

Department of Chemistry, UMIST, Manchester, M60 1QD, United Kingdom

Received: November 5, 1999

The electronic structure of the pheophytin *a* anion radical is calculated using hybrid density functional calculations at the B3LYP level. ^{1}H, ^{14}N, ^{17}O, and ^{13}C isotropic and anisotropic hyperfine couplings are calculated. Experimentally determined hyperfine couplings for ^{14}N and ^{1}H positions are in excellent agreement with theoretically calculated values. Comparison of the spin density distribution of the pheophytin radical with the related bacteriopheophytin form shows that the pheophytin radical exhibits a greater asymmetry in the distribution of spin around the ring system compared with its bacterial counterpart. In addition the delocalization of spin density onto the 3-acetyl group of bacteriopheophytin is greater than the delocalization calculated on to the corresponding vinyl group of pheophytin. This decreased delocalization for pheophytin is proposed to be responsible for the increase in electron-transfer time from the primary acceptor bacteriochlorophyll, B_A, to the secondary electron acceptor,H_A , when pheophytin replaces bacteriopheophytin in the H_A site of bacterial reaction centers. Optimal orbital overlap between B_A and H_A facilitates rapid electron transfer from B_A and may be essential in the prevention of charge recombination between B_A and the primary donor bacteriochlorophyll, D.

1. Introduction

In higher plant photosynthesis, two thylakoid membrane based reaction centers, photosystem I (PS I) and photosystem II (PS II), act in concert to transfer electrons from water to nicotinamide adenine dinucleotide phophosphate (NADP) leading to the oxidation of water to molecular oxygen and the generation of NADPH and ATP.[1] Both reaction centers use visible light energy to generate the singlet excited state of a chlorophyll *a* molecule. This energy is then used in subsequent electron transfer to effect charge transfer across the thylakoid membrane. In the PS II reaction center, the initial detected electron acceptor of the singlet excited-state electron is a pheophytin *a* molecule which becomes reduced to form a pheophytin *a* anion radical. In purple bacterial systems, a bacteriopheophytin *a* (*Rb. sphaeroides*) or a bacteriopheophytin *b* (*Rps. viridis*) molecule performs a similar role in bacterial photosynthetic electron transfer. Here, the coordinates for the heavy atoms are available form the high-resolution crystal structure determinations.[2] For the plant systems, no high-resolution crystal structures are as yet available, however from preliminary structural data, the similarity in pigment arrangement for the plant plant photosystem II and the purple bacterial systems is striking.[3]

The challenge is to understand quantitatively the electron-transfer kinetics between the different cofactors involved. Because the electron-transfer rates depend on the orientations and distances between cofactors and the electron density distribution of these cofactors, a knowledge of both the spatial *and* the electronic structure of the pigments involved is needed. While the spatial structure is available from the crystal structure data, the electronic structure will of necessity require accurate electronic structure studies for its calculation. This has been demonstrated by us recently for the bacteriopheophyin *a* anion radical formed during charge separation in the bacterial system *Rb. sphaeroides*.[4] Here, recently developed hybrid density functional calculations were used and were shown to be superior to previous approximate empirical and semiempirical calculations. Accurate electronic structure studies can work in cooperation with experimental EPR/ENDOR studies which provide complementary, albeit partial, electronic structure information from hyperfine coupling data.

In the present study, we utilize the similarity of the purple bacterial and plant PS II reaction centers to construct a model for the pheophytin *a* molecule present in PS II and also found in site modified bacterial reaction centers.[5] The electronic structure is calculated, and predicted hyperfine couplings are compared with experimental determinations. The electronic structure of the plant pigment is compared with its bacterial counterpart. Subtle electronic structure differences between the two pigments are shown to be responsible for the differences observed in experimentally measured hyperfine couplings. The role of the C3 substituent on the H_A site pheophytin molecule in facilitating rapid electron transfer from the primary acceptor chlorophyll, B_A, is explored.

2. Methods

The heavy atom coordinates for pheophytin *a* (Ph) and 3-vinyl bacteriopheophytin *b* (BPh-3v) were adapted from the coordinates of bacteriopheophytin *b* in the reaction center crystal structure of *Rps. viridis* as determined by Deisenhofer et al.[2] and obtained from the Brookhaven database (1PRC). For Ph, the saturated ring B of the bacterial pigment, Figure 1, was replaced by an unsaturated ring and methyl and ethyl substituents were added to positions 7 and 8, respectively. The acetyl group at position 3 on ring A was replaced by a vinyl group. For BPh-3v only, the acetyl group was replaced. Standard geometries for the substituted fragments were used. Hydrogens were added as described previously.[4] For computational purposes, the long phytyl chain attached to ring D was truncated to a methyl group,

10.1021/jp993907w CCC: $19.00 © 2000 American Chemical Society
Published on Web 02/15/2000

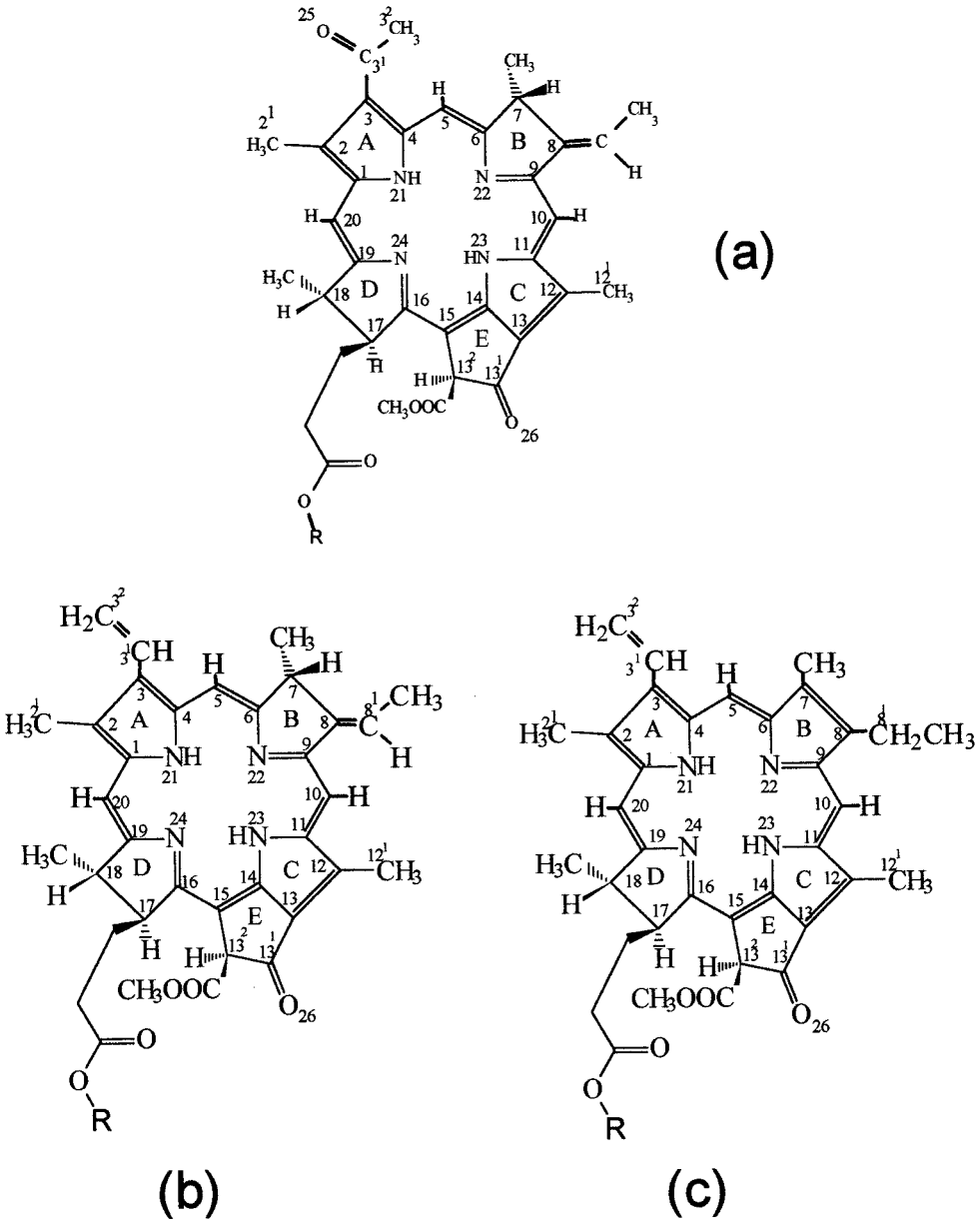

Figure 1. Molecular structures and numbering schemes of (a) bacteriopheophytin *b*, (b) 3-vinyl bacteriopheophytin *b*, and (c) pheophytin *a*. R = phytyl.

Figures 1 and 2. This is well removed from the main π electron system and will not affect the spin density distribution of the free radical. The models used are shown in Figure 2.

All density functional calculations were performed using the Gaussian 94 electronic structure code.[6] The calculations were performed at the unrestricted Kohn−Sham level and the functional used was B3LYP. The basis set was EPR-II.[4] Graphical generation of electron density surfaces was achieved using the SPARTAN package.[7]

3. Results and Discussion

The changes in molecular structure in going from the bacterial to the plant pigment are (a) the replacement of the acetyl group at the C3 position with a vinyl group and (b) the replacement of the unsaturated ring B with a saturated one. To separate out such differences, calculations were also performed on the pigment BPh-3v shown in, Figure 1b, where only the acetyl group of the bacterial pigment has been replaced by a vinyl group. The singly occupied molecular orbitals (SOMOs) of Ph, BPh-3v, and BPh are compared in Figure 3. The contour plot illustrates the similar electron density distribution for all three molecules. The most noticeable difference is the extent of the electron density surrounding atoms C4, C3, and C3[1]. For BPh, the electron density in the SOMO is located at all three atoms, whereas for both BPh-3v and Ph the electron density builds up at C4 and C3 only. Clearly, whereas delocalization onto the C3[1] atom position is extensive for an acetyl substituent at C3, this is not the case for a vinyl substituent at this position. This extra delocalization of the electron density of the SOMO for BPh compared with the other molecules will also have a stabilizing effect on the anion form of the molecule increasing its electron affinity and thereby lowering its reduction potential. Indeed, the experimentally measured redox potentials for BPh, Ph, and BPh-3v conform this trend with the BPh molecule being 140 and 160 mV less reducing than Ph and BPh-3v respectively.[8]

The more concentrated electron density contours in Figure 4 reveal differences introduced by saturation of ring B. Whereas

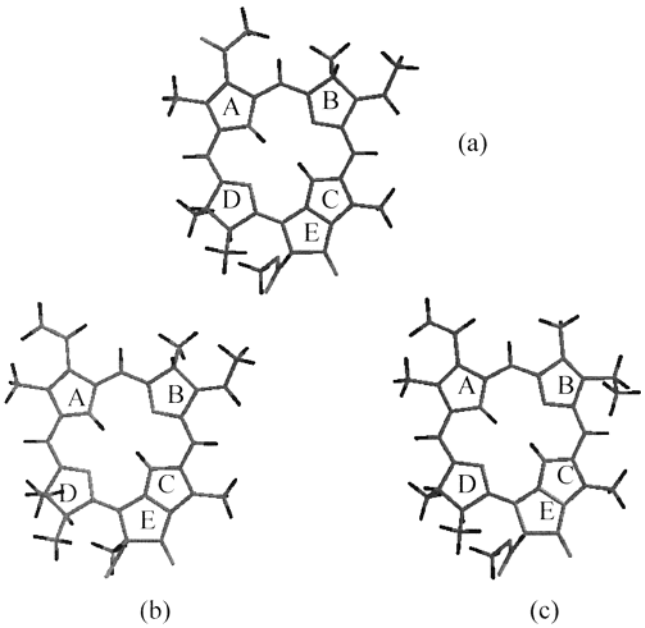

Figure 2. Truncated molecular models used for calculation purposes.

an essentially symmetrical electron density distribution is found for BPh, i.e., similar electron density at the methine positions, C5, C10, C15, and C20, and similar electron density at the C2 and C12 positions, a distinctly asymmetrical electron density distribution is noted for Ph with electron density now being concentrated at C12 relative to C2 and electron density being concentrated at the C10 methine position relative to C5, C15, and C20.

The unpaired spin density ($\alpha-\beta$) for Ph are shown in Figure 5 at a number of contour values. The contours emphasize the large spin density found at the C12 and C10 atom positions, Figure 5a. This large concentration at these positions leads to significant negative spin density at the C11 and C9 positions, parts c and d of Figure 5.

In Table 1, the anisotropic and isotropic hyperfine couplings for the three radicals are compared. An in-depth discussion of the relationship between the electron spin density distribution and the calculated anisotriopic and isotropic hyperfine couplings for BPh has been presented previously.[4] A similar relationship will exist for the two other radicals, and in this discussion we concentrate on the differences between the radical species studied. Comparing the isotropic and anisotropic hyperfine couplings for BPh and BPh-3v, Tables 1−4, shows that the major differences occur for ring A atom positions. In particular, we note that the absolute magnitude of the C2 principal anisotropic hyperfine couplings are nearly halved on replacement of the acetyl group by vinyl. The magnitude of the C1, C3, and

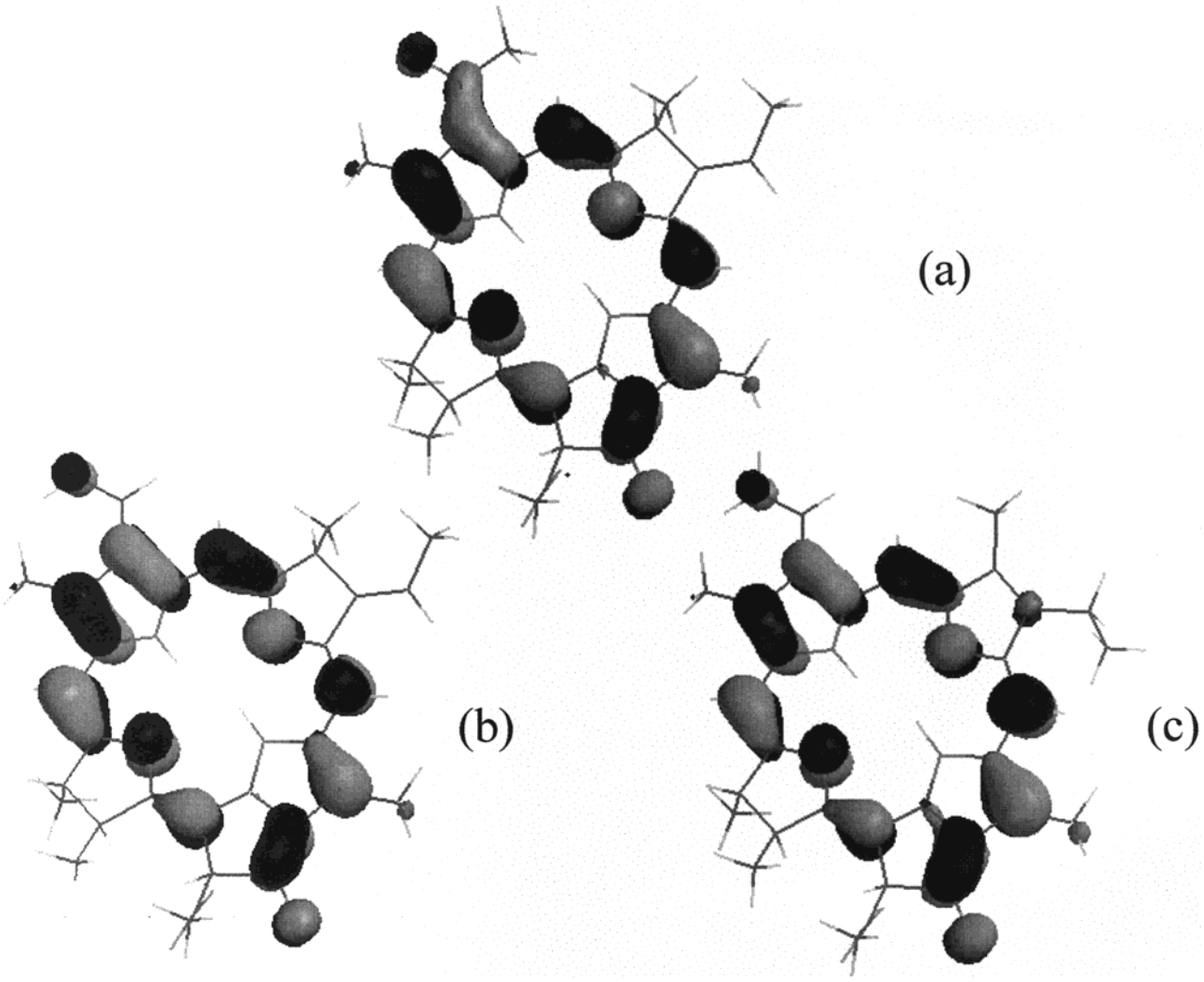

Figure 3. Singly occupied molecular orbitals (SOMOs) of (a) BPh, (b) BPh-3v, and (c) Ph.. All contours at 0.03e/au^3. Molecule orientation as in Figure 2.

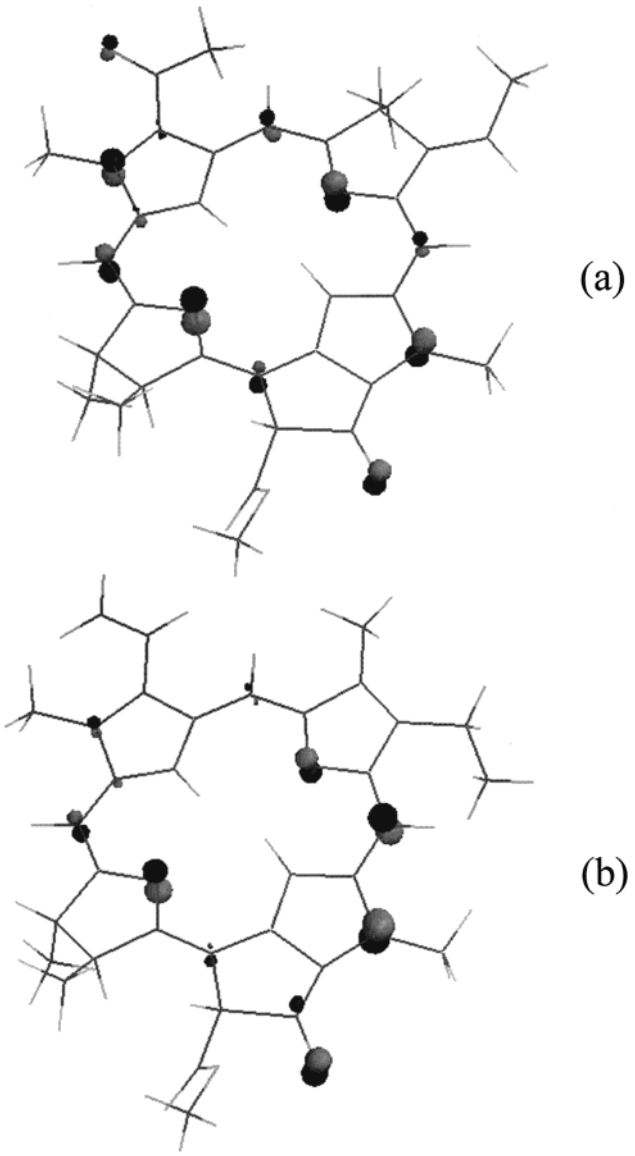

Figure 4. SOMO electron density plots at 0.09 e/au^3 for (a) BPh and (b) Ph. Molecule orientation as in Figure 2.

C4 values are increased by somewhat smaller amounts. Such variations are a direct result of the different degree of delocalization of the SOMO electron density on to the vinyl and acetyl groups for both radicals. The greater build-up of electron density on C3 and C4 in the vinyl substituted radical leads via spin polarization to an enhanced β spin at the C2 atom. This effectively reduces the spin density ($\alpha-\beta$) at this atom leading directly to the significant reduction in isotropic and anisotropic hyperfine coupling observed. Decreased spin density at C2 for 3-vinyl radicals is also manifested in the reduced C2 methyl group ^{1}H hyperfine couplings, Table 4. These protons receive spin density via hyperconjugation with the spin density at C2 and are also therefore reduced by a factor close to 2 for the 3-vinyl substituted radicals.

The affect of ring B saturation/desaturation can be examined by comparing BPh-3v with Ph in Tables 1−4. The major variations noted by this change are significantly enhanced hyperfine couplings for the C10 and C12 positions. As alluded to above the desaturation of ring B leads to a more asymmetric spin density distribution for the anion radical and this is manifested by substantially increased spin density at the C10 and C12 atom positions. This in turn leads to increases in the magnitude of the ^{1}H values for the H10 proton and the methyl group protons of C12, Table 4.

TABLE 1: ^{13}C, Isotropic (A_{iso}) and Anisotropic (T) Hyperfine Couplings Calculated for C1 to C10 (All Values Given in MHz)

	Ph		BPh-3v		BPh	
atom	T_{11} T_{22} T_{33}	A_{iso}	T_{11} T_{22} T_{33}	A_{iso}	T_{11} T_{22} T_{33}	A_{iso}
C1	9.7 −4.4 −5.4	4.7	12.0 −5.4 −6.6	4.9	8.7 −3.6 −5.1	−0.8
C2	10.2 −5.0 −5.2	0.9	12.7 −6.3 −6.5	1.6	21.3 −10.4 −10.9	7.0
C2^1	0.3 −0.1 −0.2	−2.4	0.4 −0.1 −0.3	−3.1	0.4 −0.1 −0.3	−4.6
C3	10.6 −5.2 −5.4	5.1	12.7 −6.2 −6.5	5.1	9.0 −4.1 −5.0	0.4
C3^1	1.7 1.1 −2.8	−6.1	1.9 1.1 −3.0	−6.6	3.6 −1.4 −2.2	−2.1
C3^2	7.8 −3.7 −4.1	5.3	9.0 −4.3 −4.8	5.8		-
C4	3.4 −1.4 −2.0	−2.8	5.4 −2.2 −3.2	−3.0	0.9 −0.1 −0.8	−4.8
C5	12.2 −5.9 −6.3	7.0	16.7 −8.2 −8.5	8.3	16.6 −8.1 −8.5	9.4
C6	2.6 1.3 −3.9	−9.9	2.6 1.4 −4.0	−11.5	4.0 2.7 −6.7	−12.2
C7	2.3 2.2 −4.5	−2.3	0.3 −0.1 −0.2	−0.1	0.2 −0.1 −0.2	0.5
C8	1.2 −0.4 −0.8	3.0	3.3 −1.4 −1.9	5.9	3.1 −1.3 −1.8	5.3
C8^1	0.2 −0.1 −0.2	−0.2	3.5 3.2 −6.7	−5.0	3.2 2.9 −6.0	−4.6
C9	7.0 5.3 −12.2	−18.0	6.4 4.5 −10.9	−16.7	5.5 3.8 −9.3	−15.7
C10	34.3 −16.6 −17.7	20.3	20.6 −10.0 −10.6	12.3	18.1 −8.8 −9.3	10.7

3.1. Comparison with Experimental Determinations. As mentioned in the Introduction, experimental ^{1}H ENDOR studies have been performed on the intermediate acceptor pheophytin *a* free radical of photosystem II in higher plants.[9] The principal hyperfine tensor values from the rotating methyl groups at positions 2^1 and 12^1 have been obtained. These values are given in brackets for comparison with the calculated values in Table 4. Considering the approximations of the model, the agreement between calculated values and experimentally determined ones is outstanding. ESEEM derived ^{14}N hyperfine tensors have been reported for the nitrogen atoms of the in vivo radical in ref 9c. While hyperfine tensors derived in such a fashion are often unreliable, the values reported are in reasonable agreement with those calculated in Table 3 for Ph. Extensive liquid solution studies have been performed on the pheophytin *a* anion radical and ^{1}H and ^{14}N isotropic hyperfine couplings have been determined for a number of hydrogen and nitrogen positions.[9] These are compared in Table 5 with the calculated values of this study. Clearly the conformation adapted by the free radical in solution may be different from that adopted in the in vivo environment, and this needs to be taken into account when comparing calculated and experimental values. With the above considerations taken into account, the agreement between experimental data and calculated values in Table 5 is outstanding. Of note is the enhanced magnitude of the experimentally

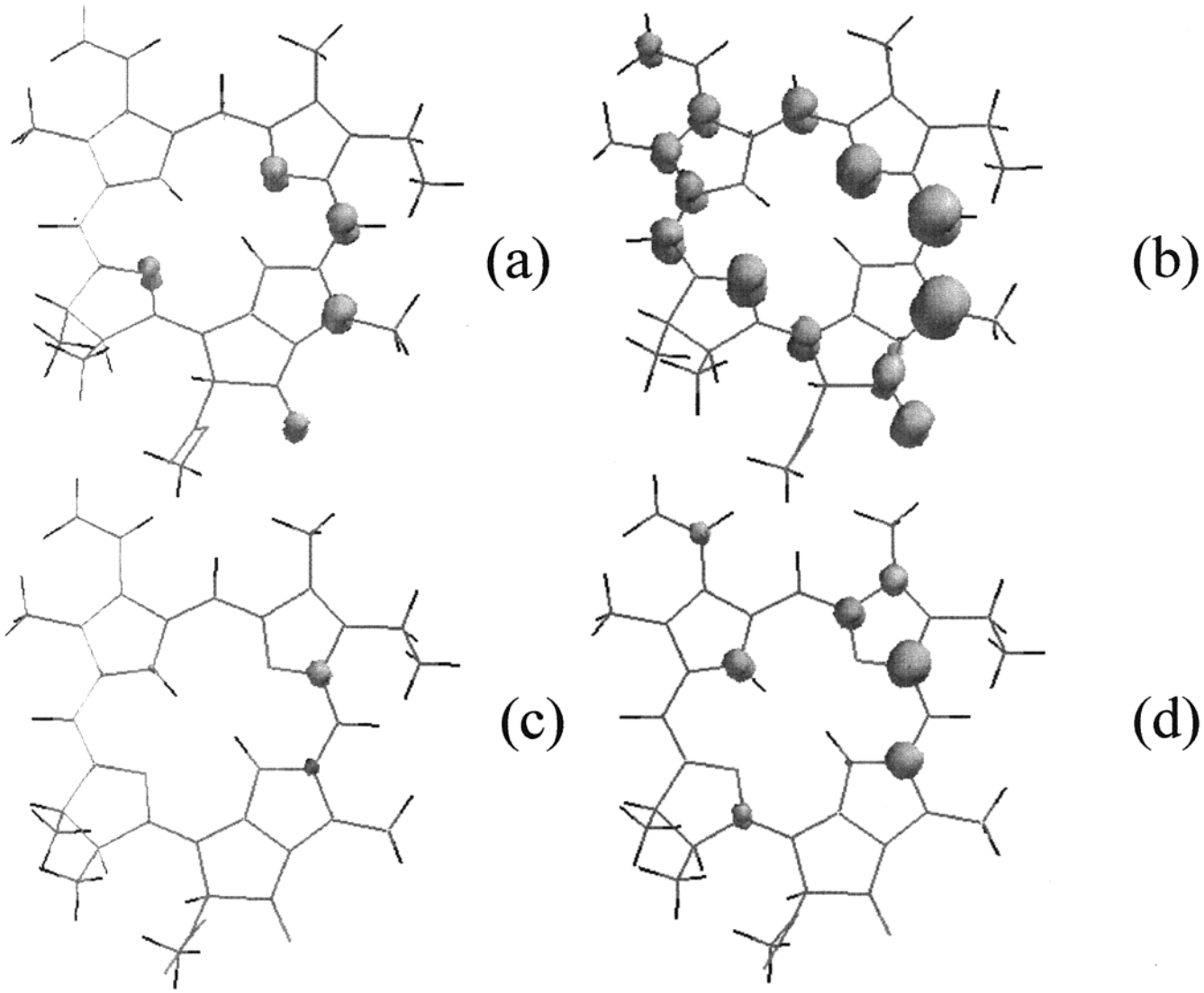

Figure 5. Unpaired spin density contours for Ph: (a) 0.05; (b) 0.01; (c) −0.002; (d) −0.0005[3] e/au[3]. Molecule orientation as in Figure 2.

measured isotropic hyperfine coupling value for the H10 proton compared with the other H5 and H20 values. This provides experimental confirmation of the asymmetric spin density distribution of pheophytin discussed on the basis of the electronic structure calculations above.

It is unfortunate that so far no ^{13}C hyperfine couplings have been reported for such radicals. Clearly, the discussion of electronic structure, based on primarily ^{1}H data, is extremely limited and interpretations on the electronic structure of such radicals based on ^{1}H data alone are likely to be speculative. More experimental effort needs to be placed on obtaining ^{13}C hyperfine couplings. Combined with the accurate prediction of such couplings now possible, Tables 1 and 2, assignment problems can be minimized enabling the electronic structure of such radicals to be probed in greater experimental detail.

3.2. Relevance to Electron Transfer. It is now widely accepted[10] that the initial electron transfer step in the *Rb. sphaeroides* and *Rps. viridis* bacterial photosynthetic reaction center proceeds from the excited singlet state of the primary donor BChl molecules (D) to another BChl molecule (B_A) in approximately 3 ps, Figure 6. The electron is then transferred in 0.9 ps (*Rb. sphaeroides*) or 0.65 ps (*Rps. viridis*) to a BPh molecule (H_A). After another 200 ps the electron is transferred to a quinone molecule. A similar reaction sequence is predicted for the photosystem II reaction center involving chlorophyll *a* and pheophytin *a* cofactors. From the crystal structure of the bacterial reaction center, the acetyl group of H_A points toward the preceding electron carrier B_A; see Figure 6. Electron transfer occurs via the lowest unoccupied molecular orbitals (LUMOs) of the cofactors which on becoming occupied during electron transfer correspond to the singly occupied molecular orbitals (SOMOs) referred to above. In our previous investigation, we have suggested that the close orbital contact caused by extension of the LUMO onto the 3-acetyl group of H_A facilitates the subpicosecond electron transfer from B_A to H_A.[4] When a vinyl group replaces the acetyl group, we would predict decreased LUMO delocalization toward the B_A chlorophyll hence reducing orbital contact between the two electron carriers. This would be expected to slow the electron transfer between the two electron carriers. Huber et al.[5] have substituted the native BPh by BPh-3v and Ph at the H_A site in *Rb. sphaeroides*. They have shown that the electron transfer from B_A to H_A slows from 0.9 ps for the native system to 1.5 ps for the substituted ones. We suggest that decreased orbital contact for B_A and H_A with BPh-3v and Ph in the H_A site can be expected to make a significant contribution to the observed slow. In addition, decreased delocalization of electron density for the SOMO of the BPh-3v and Ph radical will effectively raise the energy of $H_A(-)$ and hence raises the energy of the $B_AH_A(-)$ state relative to $B_A(-)H_A$. It was also demonstrated that the electron transfer from D

TABLE 2: ^{13}C Isotropic (A_{iso}) and Anisotropic (T) Hyperfine Couplings for C11 to C20 (All Values Given in MHz)

	Ph		BPh-3v		BPh	
atom	T_{11} T_{22} T_{33}	A_{iso}	T_{11} T_{22} T_{33}	A_{iso}	T_{11} T_{22} T_{33}	A_{iso}
C11	4.7 2.7 −7.4	−18.2	2.9 1.5 −4.3	−12.2	2.1 0.8 −2.8	−10.7
C12	36.2 −17.8 −18.4	19.8	27.1 −13.3 −13.8	14.6	25.0 −12.3 −12.7	13.3
$C12^1$	0.5 −0.2 −0.3	−7.7	0.4 −0.1 −0.2	−5.9	0.4 −0.1 −0.2	−5.5
C13	4.5 −1.3 −3.2	−6.9	5.4 −1.9 −3.5	−3.9	5.9 −2.3 −3.7	−3.1
$C13^1$	8.4 −3.6 −4.8	4.9	6.9 −2.9 −4.0	−3.7	6.2 −2.6 −3.7	2.9
$C13^2$	0.4 0.0 −0.4	−3.3	0.3 0.0 −0.3	−3.8	0.3 0.1 −0.3	−3.9
C14	1.1 0.3 −1.4	−3.1	2.0 1.5 −3.6	−5.1	2.1 1.7 −3.8	−5.5
C15	10.4 −5.0 −5.4	6.2	13.9 −6.7 −7.2	8.6	15.3 −7.4 −7.9	9.5
C16	2.2 1.1 −3.2	−6.5	3.7 2.4 −6.1	−9.3	4.0 2.6 −6.6	−10.1
C17	0.2 0.0 −0.2	0.1	0.2 0.1 −0.3	0.5	0.2 0.1 −0.3	0.5
C18	0.2 0.0 −0.2	0.5	0.3 −0.1 −0.2	0.6	0.3 −0.1 −0.2	0.8
C19	1.0 −0.2 −0.8	−5.3	1.2 −0.2 −1.0	−6.4	1.8 0.0 −1.8	−8.5
C20	11.8 −5.7 −6.1	3.0	14.6 −7.1 −7.5	4.0	17.3 −8.5 −8.9	6.1

TABLE 3: ^{17}O and ^{14}N Isotropic (A_{iso}) and Anisotropic (T) Hyperfine Couplings (All Values Given in MHz)

	Ph		BPh-3v		BPh	
atom	T_{11} T_{22} T_{33}	A_{iso}	T_{11} T_{22} T_{33}	A_{iso}	T_{11} T_{22} T_{33}	A_{iso}
N21	1.0 0.9 −1.9	−1.9	0.9 0.9 −1.8	−2.1	0.6 0.6 −1.2	−1.2
N22	11.1 −5.5 −5.7	6.0	12.8 −6.3 −6.5	6.6	11.8 −5.8 −6.0	6.2
N23	0.5 0.3 −0.8	0.4	0.3 0.2 −0.5	0.2	0.3 0.2 −0.4	0.1
N24	9.1 −4.5 −4.7	4.3	10.8 −5.3 −5.5	5.1	11.6 −5.7 −5.9	5.6
O26	−23.9 11.8 12.1	−5.7	−21.4 10.6 10.9	−5.2	−20.8 10.3 10.5	−5.0
O25					−12.9 6.4 6.5	−3.4

to B_A was slower (3.5 vs 5.8 ps) after replacement of BPh with BPh-3v at the H_A site. This was shown to be principally due to charge recombination between B_A and the primary donor bacteriochlorophyll molecules (D, Figure 6) in the substituted system. In the native system, no such back reaction is observed. This may well suggest that for the native system, subpicosecond electron transfer is needed between the first and second electron acceptors in order to separate the charges and prevent a back reaction between D and B_A. We suggest that this subpicosecond

TABLE 4: ^1H Isotropic (A_{iso}) and Anisotropic (T) Calculated Hyperfine Coupling Constants (All Values Given in MHz)[a]

	Ph		BPh-3v		BPh	
atom	T_{11} T_{22} T_{33}	A_{iso}	T_{11} T_{22} T_{33}	A_{iso}	T_{11} T_{22} T_{33}	A_{iso}
H5	3.6 −0.7 −3.0	−5.8	4.8 −1.0 −3.8	−7.3	4.5 −0.9 −3.6	−7.3
H10	8.6 −0.7 −7.9	−13.8	5.3 −0.6 −4.7	−8.8	4.7 −0.7 −4.0	−7.8
$H13^2$	0.9 0.2 −1.1	−1.3	1.0 0.1 −1.1	−0.4	1.0 0.1 −1.1	−0.1
H17	0.7 0.1 −0.8	−2.5	0.6 0.2 −0.8	−4.7	0.7 0.2 −0.8	−5.2
H18	1.0 −0.3 −0.7	−0.2	1.3 −0.4 −0.9	−0.2	1.2 −0.4 −0.8	−0.8
H20	3.5 −0.7 −2.8	−4.7	4.3 −0.9 −3.4	−5.9	4.8 −0.9 −3.9	−7.1
H21	2.5 −0.7 −1.8	1.2	2.7 −0.6 −2.2	1.0	2.3 −0.2 −2.2	0.6
H23	2.3 −0.2 −2.0	0.4	2.1 −0.1 −2.0	0.2	2.0 −0.1 −1.9	0.1

	Ph		BPh-3v		BPh	
molecule	A_{11} A_{22} A_{33}	A_{iso}	A_{11} A_{22} A_{33}	A_{iso}	A_{11} A_{22} A_{33}	A_{iso}
$CH_{3(2^1)}$	5.6 (5.6) 4.2 (4.2) 3.6 (4.2)	4.5 (4.7)	7.3 5.5 4.8	5.9		9.1
$CH_{3(12^1)}$	16.9 (14.3) 13.8 (12.1) 13.2 (12.1)	14.6 (12.8)	12.9 10.5 9.9	11.1		10.4

[a] For the methyl group protons at positions 2^1 and 12^1 the total (isotropic plus anisotropic) principal values (A) are given. These are obtained by averaging over the values calculated for a static orientation of the three hydrogens. Experimental values (9a) for the pheophytin *a* radical of photosystem II are given in brackets.

TABLE 5: Comparison of Isotropic Couplings Determined for Ph and the Isotropic Hyperfine Couplings of the Pheophytin *a* Anion Radical Determined in Dimethoxyethane[9] (All Values Given in MHz)

position	calculated	experimental
N22	6.0	6.4
N24	4.3	5.2
H5	−6.0	−7.2
H10	−13.8	−11.1
H20	−4.7	−6.2

electron transfer may well require optimal overlap of the LUMOs of B_A and H_A. This can be achieved by extension of the LUMO of H_A onto the acetyl group in the native system, which functions as an "electron density tunnel" between the two pigments. The vinyl group does not function as effectively in this regard. Recent ENDOR studies of H_A in *Rb. sphaeroides* have identified two states of reduced H_A.[11] These states were postulated to correspond to different conformations of the acetyl group at the C3 position. From the molecular orbital contours of Figure 3, it is clear that additional electron density is found along the $C3-C3^1$ bond for the reduced anion radical. Hence, the stabilization caused by planarity of this group can be expected to be higher for the anion radical form compared with the unreduced form where this orbital is unoccupied. It is quite feasible therefore that on reduction the acetyl group twists into a more favorable planar conformation maximizing electron

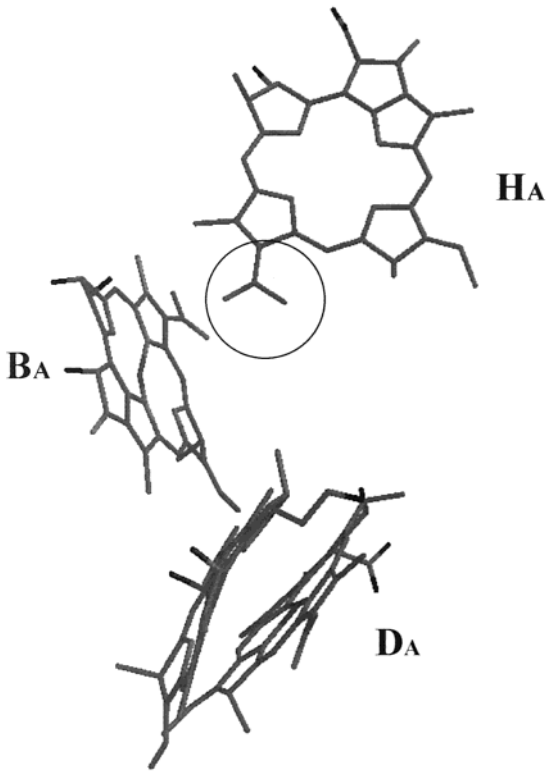

Figure 6. Spatial arrangement of the primary donor bacteriochlorophyll molecules (D), the initial electron acceptor bacteriochlorophyll molecule (B_A), and the second electron acceptor, bacteriopheophytin (H_A), as determined by Erlmer et al.[2] for the *Rb sphaeroides* reaction center. The 3-acetyl group of H_A which points toward B_A is circled.

density delocalization onto this group. At low temperatures or for short illumination times such a conformational change may not be achievable for all the centers hence accounting for the additional metastable state observed under these conditions.[11]

4. Conclusions

The electronic structure of a model pheophytin *a* anion radical has been calculated using hybrid density functional methods. Comparison of calculated hyperfine couplings with available ^1H and ^{14}N experimental determinations shows good agreement. Calculated ^{13}C hyperfine couplings provide a future reference for essential experimental studies using this nucleus. Electron density delocalization for the SOMO orbital onto the 3-vinyl group of the pheophytin radical is shown to be significantly less than that found for the corresponding 3-acetyl group of the bacteriopheophytin anion radical. This decreased delocalization is proposed to contribute to the slow in electron transfer observed between the primary electron acceptor B_A and the secondary electron acceptor H_A, when the native bacteriopheophytin is replaced by pheophytin at the H_A site of purple bacterial reaction centers. Close frontier orbital contact between the primary and secondary electron acceptors may be a prerequisite to rapidly separate the positive and negative charges generated in the primary electron-transfer event.

References and Notes

(1) (a) Brettl, K. *Biochim. Biophys. Acta* **1997**, *1318*, 322. (b) Diner, B. A.; Babcock, G. T. Structure, Dynamics and Energy Conversion Efficiency in Photosystem II. In *Oxygenic Photosynthesis: The Light Reactions*; Ort, D., Yocum, C. F., Eds.; Kluwer Academic Publishers: Dordrecht, The Netherlands, 1996; pp 137−164.

(2) (a)Deisenhofer, J.; Epp, O.; Miki, K.; Huber, R.; Michel, H. *Nature* **1985**, *318*, 618. (b) Lancaster, C. R. D.; Michel, H. Structure, **1997**, *5*, 1339. (c) Yeates, T. O.; Komiya, H.; Chirino, A.; Rees, D. C.; Allen, J. P.; Feher, G. *Proc. Natl. Acad. Sci. U.S.A.* **1988**, *85*, 8487. (d) Chang, C.-H.; Tiede, D.; Tang, J.; Smith, U.; Norris, J.; Schiffer, M. *FEBS Lett.* **1986**, *205*, 82. (e) Ermler, U.; Fritzsch, G.; Buchanan, S. K.; Michel, H. *Structure* **1994**, *2*, 925.

(3) Rhee, K.-H.; Morris, E. P.; Barber, J. *Nature* **1998**, *396*, 283.

(4) O'Malley, P. J. *J. Am. Chem. Soc.* **1999**, *121*, 3185.

(5) Huber, H.; Meyer, M.; Nagele, T.; Hartl, I.; Scheer, H.; Zinth, W.; Wachtveitl, J. *Chem. Phys.* **1995**, *44*, 55.

(6) Frisch, M. J.; Trucks G. W.; Schlegel, H. B.; Gill, P. W.; Johnson, B. G.; Wong, M. W.; Foresman, J. B.; Robb, M. A.; Head-Gordon, M.; Replogle, E. S.; Gomperts, R.; Andres, J. L.; Raghvachari, K.; Binkley, J. S.; Gonzalez, C.; Martin, R. L.; Fox, D. J.; Defrees, D. J.; Baker, J.; Stewart, J. J. P.; Pople, J. A. *GAUSSIAN 94*; Gaussian Inc.: Pittsburgh, PA, 1995.

(7) *SPARTAN 5.1*; Wave function Inc.: Irvine, CA, 1997.

(8) Geskes, C.; Meyer, M.; Fischer, M.; Scheer, H.; Heinze, J. *J. Phys. Chem.* **1995**, *99*, 17669.

(9) (a) Lubitz, W.; Isaacson, R. A.; Okamura, M. Y.; Abresch, E. C.; Plato, M.; Feher, G. *Biochim. Biophys. Acta* **1989**, *977*, 227. (b) Lendzian, F.; Moebius, K.; Lubitz, W. *Chem. Phys. Lett.* **1982**, *90*, 375. (c) Deligiannakis, H.; Rutherford, A. W. *J. Am. Chem. Soc.* **1997**, *119*, 4476.

(10) Zinth, W.; Huppmann, P.; Arlt, T.; Wachtveitl, J. *Philos. Trans. R. Soc. London, Ser. A* **1998**, *356*, 465.

(11) Mueh, F.; Williams, J. C.; Allen, J. P.; Lubitz, W. *Biochemistry* **1998**, 13066.